

Article

Conditions and Mechanism of Crystallization of Hydrous W-Fe Oxides with a Pyrochlore-Type of Structure (Elsmoreite Group) in the Oxidation Zone of Ore Deposits

Mihail Tarassov * and Eugenia Tarassova

Institute of Mineralogy and Crystallography, Bulgarian Academy of Sciences, 1113 Sofia, Bulgaria; etarassova@mail.bg

* Correspondence: mptarassov@gmail.com

Abstract: The purpose of the article is to elucidate the conditions and mechanism of crystallization of W-Fe oxide minerals with a pyrochlore-type structure (formerly ferritungstite, now elsmoreite group minerals) based on (1) a study of representative samples of secondary tungsten minerals from the oxidation zone of the Grantcharitsa tungsten deposit (Bulgaria) and (2) laboratory experiments under conditions suggested by the study of natural samples. It has been shown that crystallization of W-Fe pyrochlores occurs easily and effectively when treating $WO_3 \cdot xFe_2O_3 \cdot nH_2O$ compounds (meymacite and tungstite) with W-Fe-containing solutions with pH 2.5–6.5 (70 °C); at the same time, direct crystallization (direct low-temperature hydrothermal synthesis) of these phases from aqueous solutions is unlikely. The crystallization of W-Fe pyrochlores under natural and laboratory conditions occurs through the oriented attachment of their nanocrystals to the {111} faces of growing crystals. The nucleation of such nanocrystals occurs in the bulk of the solution as a result of the interaction of the W-Fe solution with the W-(Fe) oxide hydrate precursor. The Fe/W ratio in the resulting W-Fe pyrochlore phase depends on the Fe/W ratio in the solution and precursor, as well as on the pH of the solution.



Citation: Tarassov, M.; Tarassova, E. Conditions and Mechanism of Crystallization of Hydrous W-Fe Oxides with a Pyrochlore-Type of Structure (Elsmoreite Group) in the Oxidation Zone of Ore Deposits. *Minerals* **2024**, *14*, 422. <https://doi.org/10.3390/min14040422>

Academic Editors: Wei Tan, Xiaodong Deng, Lulu Zhao and Martin Yan Hei Li

Received: 1 April 2024
Revised: 17 April 2024
Accepted: 17 April 2024
Published: 19 April 2024



Copyright: © 2024 by the authors. Licensee MDPI, Basel, Switzerland. This article is an open access article distributed under the terms and conditions of the Creative Commons Attribution (CC BY) license (<https://creativecommons.org/licenses/by/4.0/>).

Keywords: W-Fe pyrochlore; elsmoreite group; W-Fe oxide hydrate precursor; meymacite; tungstite; particle attachment crystallization; platy and octahedral crystals

1. Introduction

Hydrous W-Fe oxides with a pyrochlore-type structure occur in nature as secondary tungsten minerals resulting from the alteration of scheelite and minerals of the wolframite series and belong to the elsmoreite group of the pyrochlore supergroup of minerals with the general formula $A_{2-m}B_2X_{6-w}Y_{1-n}$ [1]. In the formula of the elsmoreite group, *A* is a vacancy, H_2O , or a large 8-coordinated cation with a radius of $\sim 1.0 \text{ \AA}$ (Na^+ , Ca^{2+} , Pb^{2+} , Bi^{3+}); *B* is a 6-coordinated high field-strength cation (W^{6+}) and Fe^{3+} and Al^{3+} ; *X* is O^{2-} and OH^- ; *Y* is a vacancy, H_2O , OH^- , and a very large ($\gg 1.0 \text{ \AA}$) monovalent cation (K^+ , Cs^+) [1–3]. To date, the elsmoreite group of minerals includes the following: (1) hydroknoelsmoreite (formerly known as ferritungstite and alumotungstite until 2010; discredited), which is the most common representative of the elsmoreite group and has a variable composition—from pure tungsten oxide hydrate $\square_2W_2O_6 \cdot H_2O$ [4] to varieties with dominant H_2O and vacancies at the *Y* and *A* sites, respectively, but with a significant presence of other cations at the *A*, *B*, *X*, and *Y* sites giving the formula $(\square, Na^+, Ca^{2+}, Pb^{2+}, Bi^{3+}, H_2O)_{\Sigma 2}(W, Fe^{3+}, Al)_{\Sigma 2}(O, OH)_{\Sigma 6}(H_2O, \square, K, Cs)_{\Sigma 1}$, [1]; (2) hydroxyknoelsmoreite, $(\square, Pb^{2+}, Ca^{2+}, Na^+, K^+, Ba^{2+})_{\Sigma 2}(W, Fe^{3+}, Al)_{\Sigma 2}(O, OH)_{\Sigma 6}(OH)$, with dominant OH and vacancies in the *Y* and *A* sites, respectively [3]; and (3) hydroplumboelsmoreite (formerly jixianite), $(Pb_1 \square_1)_{\Sigma 2}(W_{1.33}Fe^{3+}_{0.67})_{\Sigma 2}O_6(H_2O)$ with dominant H_2O and Pb at the *Y* and *A* sites, respectively [5].

Minerals of the elsmoreite group are quite typical products of supergene processes in the oxidation zones of tungsten and tungsten-containing deposits, although they can also form as products of hydrothermal alteration of primary tungsten minerals [6]. Data on the chemical composition and structure of this group of minerals have long been controversial due to the very small size of the crystals, the presence of fine mixtures with other secondary minerals, and the state of analytical methods used in the past.

The mineral hydrokenoelsmoreite was first described under the name “ferritungstite” by W.T. Schaller in 1911 for tungstic ocher resulting from the oxidation of wolframite in the Germania tungsten mine in the State of Washington, USA [7]. The mineral was described as platy hexagonal crystals of “a hydrous ferric tungstate” with a formula $\text{Fe}_2\text{O}_3 \cdot \text{WO}_3 \cdot 6\text{H}_2\text{O}$ ($\text{Fe}/\text{W} = 2$). A later study of the original Schaller sample [8], interpreted by [9], showed that Schaller ferritungstite is rather a mixture of ferritungstite and jarosite and that the atomic Fe/W ratio of ferritungstite is <2 . The use of electron probe microanalysis to study minerals of the elsmoreite group, particularly in articles published in the last 30 years, shows that the Fe/W or $(\text{Fe} + \text{Al})/\text{W}$ atomic ratios in these minerals are significantly less than unity. If we exclude the unique composition of hydrokenoelmorite $\square_2\text{W}_2\text{O}_6 \cdot \text{H}_2\text{O}$ described in [4], then, according to most researchers [2,3,5,10–14] the ratio $(\text{Fe} + \text{Al})/\text{W}$ is not strictly fixed and varies within the range of 0.27–0.51.

Van Tassel [15] was the first to point out that the structure of hydrokenoelsmoreite (ferritungstite) belongs to a pyrochlore-type structure. This finding was conclusively confirmed by single-crystal X-ray diffraction of a mineral from Kalsas Mountain, Yukon, performed by [2]. According to [13], hydrokenoelsmoreite occurs in two polytypes: hydrokenoelsmoreite-3C (S.G. Fd-3m) and hydrokenoelsmoreite-6R (S.G. R-3). The structures of other members of the elsmoreite group are described within the space groups Fd-3m (hydroplumboelsmoreite) [5] and R-3 (hydroxykenoelsmoreite) [3].

The conditions and mechanism of crystallization of minerals of the elsmoreite group still remain practically unstudied. It is well known that the minerals of this group are formed as a result of the alteration of primary tungsten minerals. But at what stage of the alteration of primary minerals and, in general, at what stage of the geochemical evolution of tungsten (for example, in the oxidation zone of ore deposits) the elsmoreite group of minerals is formed is not completely clear.

Minerals of the elsmoreite group can occur as incrustations and fillings both in the cavities of primary minerals, such as ferberite [2,6,15], and outside the location of primary minerals, for example, in cavities in quartz [4]. In these incrustations, in addition to the elsmoreite group, other secondary tungsten minerals are often present, which makes it difficult to determine the sequence of formation of secondary tungsten minerals. Cases of direct replacement of primary tungsten minerals by minerals of the elsmoreite group of minerals are very rare. In these cases, questions arise as to whether the described mineral belongs to the elsmoreite group and whether direct replacement of the primary mineral actually occurs. Matsubara [10] describes the direct replacement of scheelite by dense aggregates of hydrokenoelsmoreite (ferritungstite). But, the 12% water content reported in this paper is atypically high for ferritungstite, which is close to that of the amorphous mineral meymacite. The microtexture of this replacement also corresponds to the replacement of scheelite with iron-containing meymacite [16]. Sahama [6] described pseudomorphs of platy ferritungstite after scheelite, which, however, correspond more to the filling of a cavity after the dissolution of scheelite than to its direct replacement.

There is evidence that the minerals of the elsmoreite group are not formed directly during the destruction of the primary minerals but at a later stage at the expense of earlier alteration products. Among such earlier products of alteration of primary tungsten minerals and precursors of minerals of the elsmoreite group are Fe and Mn containing hydrotungstite $\text{WO}_3 \cdot 2\text{H}_2\text{O}$ replacing hübnerite [11]; anthoinite $\text{AlWO}_3(\text{OH})_3$ and mpororoite $\text{Al}_2\text{O}(\text{WO}_4)_2 \cdot 6\text{H}_2\text{O}$ pseudomorphically replacing scheelite [14]; meymacite $\text{WO}_3 \cdot 2\text{H}_2\text{O}$ and Fe-containing meymacite $\text{WO}_3 \cdot x\text{Fe}_2\text{O}_3 \cdot n\text{H}_2\text{O}$ replacing scheelite [15,16].

Some data on the possible conditions of crystallization of minerals of the elsmoreite group can be derived from the conditions of synthesis of artificial tungsten pyrochlores. Synthetic tungsten-based pyrochlore oxides have long been the focus of scientific interest due to their promising electrochemical properties for use in electrochemical devices (lithium batteries and electrochromic windows) [17] and for photocatalytic applications in energy (solar water splitting) and environmental protection (purification) [18,19]. Among the methods used for the synthesis of tungsten pyrochlores (solid-phase synthesis, hydrothermal synthesis, solvothermal synthesis, coprecipitation + annealing, etc.), hydrothermal synthesis (usually at temperatures > 100 °C) is more consistent with the natural conditions for the formation of elsmoreite group minerals. The pH = 3 of solutions used in the direct synthesis at 155 °C of the artificial hydrokenoelsmoreite analog $\square_2\text{W}_2\text{O}_6 \cdot \text{H}_2\text{O}$ [20] is sometimes cited as a likely pH parameter for the formation of natural hydrokenoelsmoreite. As far as we know and according to [9], the first documented attempts, although unsuccessful, to obtain hydrokenoelsmoreite (ferritungstite) in laboratory conditions were made by Graf D.L. in his Master's Thesis (1947). It is assumed that as a basis for his research, the author used the chemical composition of ferritungstite proposed by Schaller [7].

The present work aims to elucidate the conditions and mechanism of crystallization of W-Fe minerals of the elsmoreite group based on (1) the detailed examination of representative samples of secondary tungsten minerals from the oxidation zone of the Grantcharitsa tungsten deposit (Bulgaria) and (2) laboratory experiments under conditions suggested by the study of natural samples. All laboratory experiments were performed at 70 °C, which is the lowest temperature for synthesis of tungsten pyrochlore known so far.

The authors believe that the results of this study can be applied to the oxidation zones of other tungsten deposits. The oxidation zone of the Grantcharitsa tungsten deposit is considered by the authors as a representative site in which the mineral formation in the $\text{WO}_3\text{-Fe}_2\text{O}_3\text{-H}_2\text{O}$ system takes place, including the formation of hydrokenoelsmoreite. This is due to the fact that the primary ore mineralization is represented by a stable association of pyrite and scheelite in pegmatoid quartz-feldspathic veins, with a subordinate amount of other ore minerals. The deposit is located in porphyry biotite granites and amphibole-biotite granodiorites from the so-called "unit 1" (66.79 ± 0.29 Ma) of the composite Rilo-Western Rhodope batholith [16].

2. Materials and Methods

2.1. Geological Materials

Representative samples taken from the oxidation zone of the Grantcharitsa deposit, Western Rhodopes Mountains, Bulgaria, were used for the present study. The samples were selected to more clearly visualize and interpret the relationships between natural W-Fe pyrochlore–hydrokenoelsmoreite with primary scheelite and other secondary tungsten minerals and to show the place of hydrokenoelsmoreite in the geochemical evolution of tungsten in the oxidation zone of the deposit.

2.2. Laboratory Experiments

Iron (III) sulfate hydrate $\text{Fe}_2(\text{SO}_4)_3 \cdot x\text{H}_2\text{O}$ (97%) ($x = 6.034$ measured by TG analysis) and sulfuric acid H_2SO_4 (95%–97%) (reag. Ph. Eur) of Sigma-Aldrich and analytical grade sodium tungstate dihydrate $\text{Na}_2\text{WO}_4 \cdot 2\text{H}_2\text{O}$ and hydrochloric acid HCl (37%) were used in laboratory experiments. The reagents were selected to better suit the chemical environment of the oxidation zone of the W-containing sulfide deposit, in which the presence of Fe, sulfate ions, and sulfuric acid in supergene solutions is mainly associated with the oxidation of pyrite.

All experiments were carried out at 70 °C in an MTA Kutesz shaker thermostat using 25–50 mL aqueous solutions with a W concentration of 0.05 M, variable Fe concentrations ensuring an atomic Fe/W ratio of 0–0.5 in solution, and with different pH values. The choice of the temperature of 70 °C was dictated by the low rates of equilibration of the iso- and heteropolytungstate anions in aqueous solutions at room temperature. At room

temperature, these equilibria can be reached in hours or weeks, especially in the pH range ($\text{pH} < 5$) where metatungstate ions are formed [21]. The pH measurements of the solutions were performed before and after experiments at room temperature using a Radelkis OP-211/1 digital pH meter and a Thermo Scientific Orion Star A329 portable pH/conductivity/DO meter.

Two types of experiments were performed as follows: (1) direct hydrothermal synthesis within a $\text{WO}_3\text{-Fe}_2\text{O}_3\text{-H}_2\text{O}$ system; (2) transformation of solid precursors ($\text{WO}_3 \cdot x\text{Fe}_2\text{O}_3 \cdot n\text{H}_2\text{O}$, $\text{WO}_3 \cdot \text{H}_2\text{O}$) by treating them with W-Fe solutions at different pH.

2.2.1. Direct Hydrothermal Synthesis

The synthesis was conducted for two series of solutions with Fe/W atomic ratios of 0.1 and 0.5, each series consisting of 8 solutions with different pH values ranging between 0.5 and 4.0. Preparation of the solutions involved the following steps: (1) dissolving $\text{Fe}_2(\text{SO}_4)_3 \cdot x\text{H}_2\text{O}$ in deionized water to obtain 50 mL of 0.0132 M or 0.00264 M $\text{Fe}_2(\text{SO}_4)_3$ solution; (2) addition of 2.6 mL of 1 M Na_2WO_4 ; (3) gradual addition of H_2SO_4 with a concentration of 2 M, 1 M, or 0.5 M to adjust the pH of the solutions with an approximate step of 0.5. All these operations were carried out at room temperature, using an electromagnetic stirrer and simultaneously determining the pH of the solution with a pH meter. A part of the obtained solutions contained white to beige suspensions. Then, sealed flasks with the solutions were placed in a shaker thermostat at a temperature of 70 °C for 400 h. After the experiments, the pH of all solutions was again measured at room temperature; the precipitates were filtered and washed with deionized water and acetone and then dried at 50 °C.

2.2.2. Treatment of Solid Precursors with W-Fe Solutions

The experiments involved the preparation of a series of precursors:

(a) Amorphous gels of W-Fe oxide hydrate ($\text{WO}_3 \cdot x\text{Fe}_2\text{O}_3 \cdot n\text{H}_2\text{O}$) (artificial chemical analogs of meymacite) with different Fe/W atomic ratios (0.10–0.23) using different molar proportions of Na_2WO_4 , $\text{Fe}_2(\text{SO}_4)_3$ and H_2SO_4 at room temperature (Table S1); and (b) $\text{WO}_3 \cdot \text{H}_2\text{O}$ (analogs of tungstite—common mineral in the oxidation zones of ore deposit [6]) prepared by Freedman's method [22] at 100 °C and via the decomposition of scheelite with sulfuric acid at 110 °C. The experiments involved sequentially performing the following steps:

(1) Preparation of 25 mL batches of $\text{Fe}_2(\text{SO}_4)_3 + \text{H}_2\text{SO}_4$ solutions of various concentrations at room temperature. To prepare solutions with a target Fe/W ratio of 0.10, 0.11, 0.3, and 0.5, the following volumes of 0.05 M $\text{Fe}_2(\text{SO}_4)_3$ were used—1.32, 1.45, 3.96, and 6.6 mL, respectively. To these volumes, the required volumes of 0.1 M H_2SO_4 were then added, as determined experimentally (for the planned pH range of 3–7 for a solution of Fe/W = 0.1, volumes of 0.1 M H_2SO_4 ranged from 8.5 to 6.5 mL). Deionized water was then added to make up the solution to 25 mL.

(2) Addition of 1.32 mL 1 M Na_2WO_4 to each solution in step 1, thereby forming a series of working solutions with a total tungsten concentration of 0.05 M and varying Fe/W and pH.

(3) Placing the working solutions in a thermostat at 70 °C for 1–5 days (to achieve equilibria in the solutions); then, the pH of the solution was measured at room temperature.

(4) To the prepared working solutions in step 3, solid precursors were added (about 0.01–0.02 mole of W recalculated to the volume of the solution). For better interaction with the solutions, all precursors were previously ground in a mortar. Then, the working solutions with the solid precursors were placed in a thermostat at 70 °C for a period of 2–3 weeks. After the experiment, the pH of the solutions was measured at room temperature and filtered, and the solid material was washed with deionized water and dried at 50 °C.

2.3. Methods

Scanning electron microscopy (SEM) and energy dispersive X-ray (EDX) analysis (ZEISS EVO LS25—EDAX Trident) were applied to investigate the morphology and chemical composition of natural and artificial materials. For this purpose, part of the sample grains was directly attached to SEM stubs, while another part was embedded in epoxy resin and then polished, and both types of specimens thus obtained were coated with carbon. SEM-EDX was performed at an accelerating voltage of 15 kV using an EDAX SDD Apollo 10 EDS detector and a Genesis V. 6.2. software with ZAF correction method and hematite (for Fe), scheelite (W), albite (Na), sanidine (K), crocoite (Pb), and anhydrite (S) as reference standards. A part of the natural W-Fe pyrochlores (hydrokenoelsmoreite) from the Grantcharitsa deposit was studied by high-resolution TEM at 120 kV using a transmission electron microscope Philips TEM420. The phase composition of the materials was examined using powder X-ray diffraction analysis on a PANanalytical EMPYREAN diffractometer system ((IMC-BAS), Cu anode, 45 V, 40 mA, range 3–100 degrees 2Theta, step size 2Theta—0.0130).

3. Results

3.1. Formation of Hydrokenoelsmoreite in the Grantcharitsa Deposit

3.1.1. Scheelite Alteration and Role of Meymacite

A thorough examination of samples with scheelite and secondary tungsten minerals showed that there was not a single case of direct replacement of scheelite with hydrokenoelsmoreite. In this work, we confirm our earlier conclusion [16] that iron-containing meymacite $\text{WO}_3 \cdot x\text{Fe}_2\text{O}_3 \cdot n\text{H}_2\text{O}$ ($x = 0.12\text{--}0.25$, $n = 1.8\text{--}3.9$) is the first supergene product of scheelite alteration and the most common secondary tungsten mineral at the deposit. The mineral forms partial or complete pseudomorphs after scheelite and often shows oriented penetration into scheelite crystals (Figure 1a,b). The earliest formed meymacite has a lower content of iron and water ($x \approx 0.12$, $n \approx 1.8$), and due to later processes—aging and interaction with supergene solutions—its chemical composition changes.

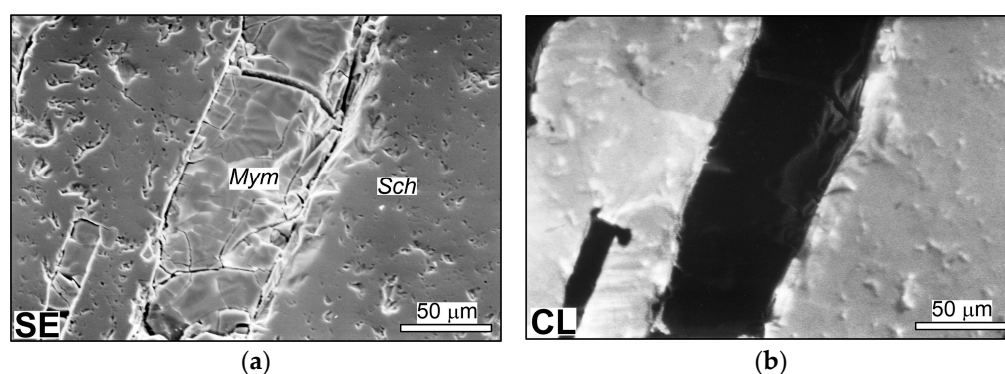


Figure 1. Crystallographically oriented pseudomorphic replacement of scheelite (*Sch*) by Fe-containing meymacite (*Mym*): (a) image in secondary electrons (SE); (b) image in cathode luminescence (CL).

The mineral has a resinous to glassy luster and a color of varying shades of yellow and brown—from light-yellow to dark- and black-brown—and according to these characteristics, it corresponds to the first description of meymacite, made in 1874 by A. Carnot [23]. It should be noted that A. Carnot’s meymacite also contained iron, which, however, the author attributed to mechanical impurities of other minerals. According to [15,23] and the existing nomenclature, meymacite is considered an amorphous analog of hydrotungstite, $\text{WO}_3 \cdot 2\text{H}_2\text{O}$. Our investigation [16] showed that meymacite from the Grantcharitsa deposit actually is a nanocrystalline material, the most ordered parts of which are represented by filamentous nanocrystals 20–25 nm long and 2–3 nm wide with the structure of $\text{WO}_3 \cdot 1/3\text{H}_2\text{O}$ (S.G. Fmm2, $a = 7.359 \text{ \AA}$, $b = 12.513$, $c = 7.704$) [24]. The nanocrystals are elongated in [001]

direction. The $\text{WO}_3 \cdot 1/3\text{H}_2\text{O}$ structure consists of layers of corner-sharing WO_6 octahedra forming six-membered rings characteristic by hexagonal WO_3 and hexagonal tungsten bronzes (HTB). Layers are stacked in the [001] direction, with each layer being displaced by $a/2$ relative to the adjacent layer.

The special place and significance of meymacite in the oxidation zone of the Grantcharitsa deposit is that it is the precursor of all other minerals, including hydrokenoelsmoreite. The possible path and conditions of decomposition and replacement of scheelite by iron-containing meymacite as well as the possible paths and conditions of alteration of meymacite in the Grantcharitsa deposit can be inferred using the Eh-pH diagrams for the W-Ca-Fe-S-K-O-H (Figure 2a) and W-Fe-S-K-O-H (Figure 2b) systems constructed by us in [16] and modified for this study. The selected activities of the chemical components (Fe, Ca, S, and K) in aqueous solutions correspond to those in the oxidation zones of the ore deposits, and the activity for W corresponds to the scheelite solubility [16].

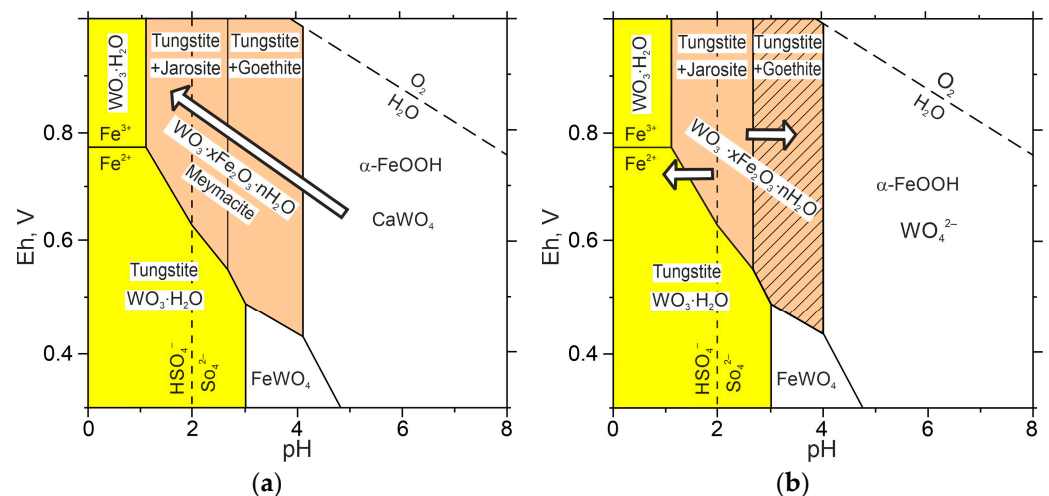


Figure 2. (a) Pathway of alteration of scheelite and formation of meymacite in Eh-pH diagram of the W-Ca-Fe-S-K-O-H system ($\Sigma\text{Fe}—10^{-4}$, $\text{Ca}^{2+}—10^{-4}$, $\Sigma\text{S}—10^{-2}$, $\text{K}^+—10^{-3}$; 298 K, 1 atm.). (b) Pathways of alteration of meymacite in Eh-pH diagram of the W-Fe-S-K-O-H system (according to [16] with corrections) ($\Sigma\text{Fe}—10^{-4}$, $\text{Ca}^{2+}—10^{-4}$, $\Sigma\text{S}—10^{-2}$, $\text{K}^+—10^{-3}$; W monomeric— 10^{-5} ; 298 K, 1 atm.).

3.1.2. Meymacite—Hydrokenoelsmoreite Relationships

All other identified secondary tungsten minerals and tungsten-bearing minerals in the deposit (tungstite, hydrotungstite, hydrokenoelsmoreite, stolzite, supergene scheelite, W-bearing hematite, and W-bearing goethite) are clearly secondary to meymacite. The minerals tungstite, hydrotungstite, and hydrokenoelsmoreite are formed at the expense of meymacite and in place of meymacite while other minerals are not spatially associated with meymacite. Before its transformation into other secondary minerals, meymacite undergoes significant changes associated with the aging of the mineral as a natural gel [25]. As a result, primary glassy meymacite retains a stable glassy base (skeleton) and cavities occupied by gel aging products, such as spongy aggregates (Figure 3a), which are the most ordered part of meymacite [16].

It is in these cavities in meymacite that hydrokenoelsmoreite (Figure 3b,c) and another secondary tungsten mineral—hydrotungstite, $\text{WO}_3 \cdot 2\text{H}_2\text{O}$, stable at $<50^\circ\text{C}$ (Figure 3d)—are formed. Hydrotungstite occurs as bright-yellow aggregates of crystals with a size of 50–60 μm . Hydrokenoelsmoreite occurs as yellow to grey-brownish aggregates of smaller crystals (5–20 μm) with a strong diamond luster. The conditions for the transformation of meymacite into these two minerals are fundamentally different, and the Eh-pH diagram we constructed in Figure 2b can be used to assess these conditions. It follows that the formation of hydrotungstite (tungstite) occurs as a result of the interaction of sulfuric acid solutions ($\text{pH} < 1$) with meymacite. The succession of the minerals scheelite—Fe-containing

meymacite—and hydrotungstite (tungstite) reflects the general tendency of the evolution of mineral forms of tungsten in the oxidation zone of the Grantscharitsa deposit when the pH of the supergene solutions decreases. Hydroknoelsmoreite is out of this tendency.

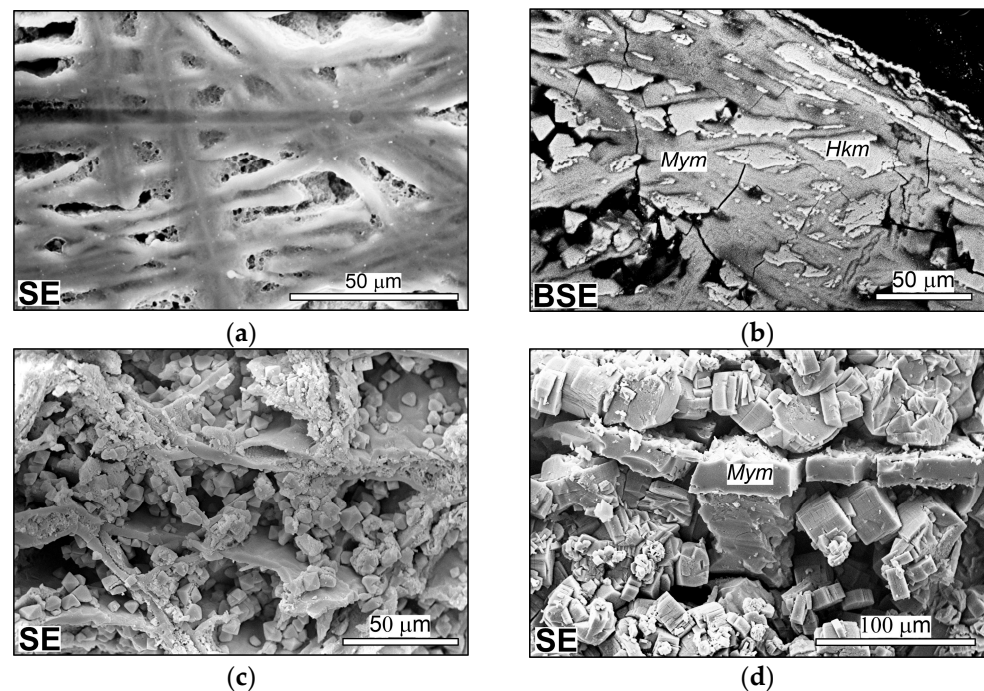


Figure 3. SEM images illustrating relationships between meymacite and hydroknoelsmoreite and hydrotungstite: (a) Meymacite microstructure (cavities, empty or filled by spongy aggregates in glassy material) as result of aging (polished section); (b) development of hydroknoelsmoreite after meymacite—filling the cavities in meymacite (polished section); (c) incrustation of octahedral crystals of hydroknoelsmoreite on the walls of cavities in meymacite; (d) development of hydrotungstite, $\text{WO}_3 \cdot 2\text{H}_2\text{O}$ after meymacite (relics of meymacite glassy skeleton are in the center of the image). *Mym*—meymacite; *Hkm*—hydroknoelsmoreite.

It has been established that meymacite in samples containing hydroknoelsmoreite is distinguished by a number of features: (1) the relative volume of cavities in meymacite increases sharply; in some cases, only skeletal walls 3–5 μm wide are preserved (Figure 3c); (2) the material becomes very fragile and friable. The formation of hydroknoelsmoreite also causes a significant change in the composition of meymacite (Table 1); the contents of Fe_2O_3 and H_2O increase and those of WO_3 decrease (analyses 2 and 4) in comparison with meymacite without hydroknoelsmoreite (analysis 1). The latter analysis is related to the most common variety of meymacite in the Grantcharitsa deposit.

Fragility in combination with the increased content of water indicates increased porosity of meymacite, which, together with an increase in the volume of cavities in the mineral, indicate that during the crystallization of hydroknoelsmoreite, meymacite is intensively dissolved by supergene solutions. This process occurs when the pH of the supergene solution increases. The field (tungstite + goethite) of the Eh–pH diagram (Figure 2b) can, to a first approximation, be taken as the conditions for the crystallization of hydroknoelsmoreite ($\text{pH} \approx 3\text{--}4$).

A change in the pH regime of supergene solutions may reflect the staged development of processes in the oxidation zone and is associated mainly with the depletion of sulfides, the oxidation of which ensures the formation of natural sulfuric acid [26]. The acidity of supergene solutions is also gradually neutralized as a result of the interaction of sulfuric acid with scheelite and silicate minerals (quartz, microcline, albite, and biotite), which leads to a simultaneous increase in the concentration of potassium and sodium. The chemical composition of the coexisting pairs of meymacite—hydroknoelsmoreite (Table 1) suggests

that the supergene solution that caused the formation of hydroknoelsmoreite contained Na, K, Ca, W, and Fe.

Table 1. Representative EDX analyses of meymacite and hydroknoelsmoreite (wt.%) and their crystal chemical formulas.

N ^o an.	Mineral	WO ₃	Fe ₂ O ₃	Na ₂ O	K ₂ O	CaO	H ₂ O ¹	Fe/W at. Ratio
1	meymacite	79.0	7.9	-	-	0.6	12.5	0.29
2 ²	meymacite	74.7	9.1	-	0.1	0.3	15.8	0.35
3 ²	hydroknoelsmoreite	81.2	9.3	1.4	1	0.3	6.8	0.33
4 ³	meymacite	70.4	10.9	-	-	0.1	18.6	0.45
5 ³	hydroknoelsmoreite	79.9	9.5	1.0	1.2	0.2	8.2	0.35

Chemical formulas/crystal chemical formulas

1. WO₃·0.145Fe₂O₃·0.031CaO·2.036H₂O

2. WO₃·0.177Fe₂O₃·0.017CaO·0.003K₂O·2.722H₂O

3. (□_{1.657}Na_{0.194}(H₂O)_{0.126}Ca_{0.023})_{Σ2}(W_{1.501}Fe³⁺_{0.499})_{Σ2}(O_{4.835}(OH)_{1.165})_{Σ6}((H₂O)_{0.909}K_{0.091})_{Σ1}

4. WO₃·0.225Fe₂O₃·0.006CaO·3.400H₂O

5. (□_{1.402}(H₂O)_{0.444}Na_{0.139}Ca_{0.015})_{Σ2}(W_{1.487}Fe³⁺_{0.513})_{Σ2}(O_{4.741}(OH)_{1.259})_{Σ6}((H₂O)_{0.890}K_{0.110})_{Σ1}

¹ The difference between 100% and the sum of the analysis. ^{2,3} Coexisting pairs meymacite—hydroknoelsmoreite.

3.1.3. Morphology of Hydroknoelsmoreite and Peculiarities of Its Surface

Hydroknoelsmoreite of the Grantcharitsa deposit occurs in the form of well-faceted octahedral crystals, their twins, and intergrowths according to the spinel law. Besides dominant octahedral faces {111}, hydroknoelsmoreite crystals rarely have cube faces {100}. Individual crystals are rare. The mineral usually occurs in the form of aggregates of intergrown crystals. The predominant part of the crystals demonstrates a specific granular (mosaic) structure on their {111} faces (Figure 4a,b). The grains are round or with hexagonal contours. Their size is ≤1 μm and varies from sample to sample; for example, it is 0.5–1.0 μm for the sample in Figure 4a and 0.1–0.2 μm for the sample in Figure 4b. This feature of the crystal faces can serve as an indication that the crystallization of hydroknoelsmoreite occurs through the mechanism of “particle attachment” [27] or “oriented attachment of particles” [28]. This crystallization mechanism has been proposed for tungsten pyrochlore obtained in hydrothermal treatment experiments at 180 °C [29] and for synthetic tungstite obtained at 100 °C [30].

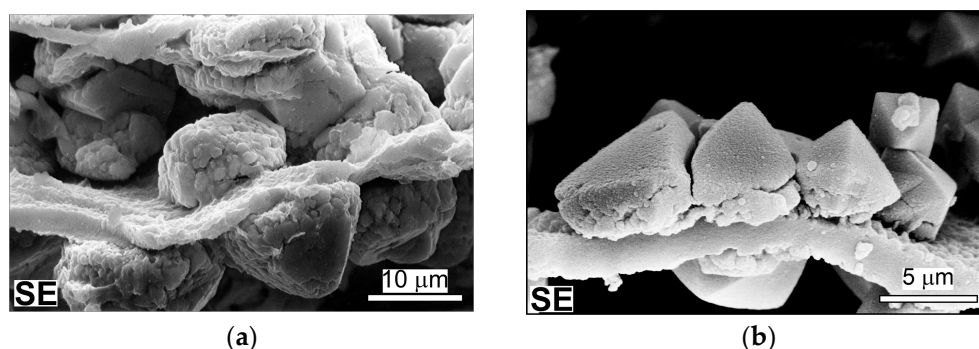


Figure 4. SEM images of hydroknoelsmoreite octahedral crystals whose {111} faces demonstrate granular (mosaic) structure as a result of crystallization by particle attachment [27,28]: (a) octahedral crystals 10–15 μm in size with surface grains of 0.5–1.0 μm; (b) octahedral crystals 5–9 μm in size with surface grains of 0.1–0.2 μm.

3.1.4. TEM Study of Hydroknoelsmoreite

TEM study was used in this study to obtain more detailed information about the structure of the grains that make up the granular structure on the {111} faces (Figure 4a,b). A thin fragment of one of such grains, 0.3 μm wide, is shown in Figure 5a. The particle

is oriented along the [112] direction. The bright-field image in Figure 5a shows the particle's inhomogeneity and defect structure in diffraction contrast (visible as a granular structure). The selected area of the electron diffraction pattern (insert in Figure 5a) confirms the inhomogeneity of the particle: a part of the spot reflections is arc-shaped; there are additional extra reflections. Arc-shaped reflections indicate that local areas (domains) in the particle are rotated relative to each other at an angle of 3–4°. Of the extra reflections in the pattern, the most important are those that correspond to the [112] zone. For example, the experimental pattern demonstrates reflection (1–10), which is forbidden for the space group Fd-3m.

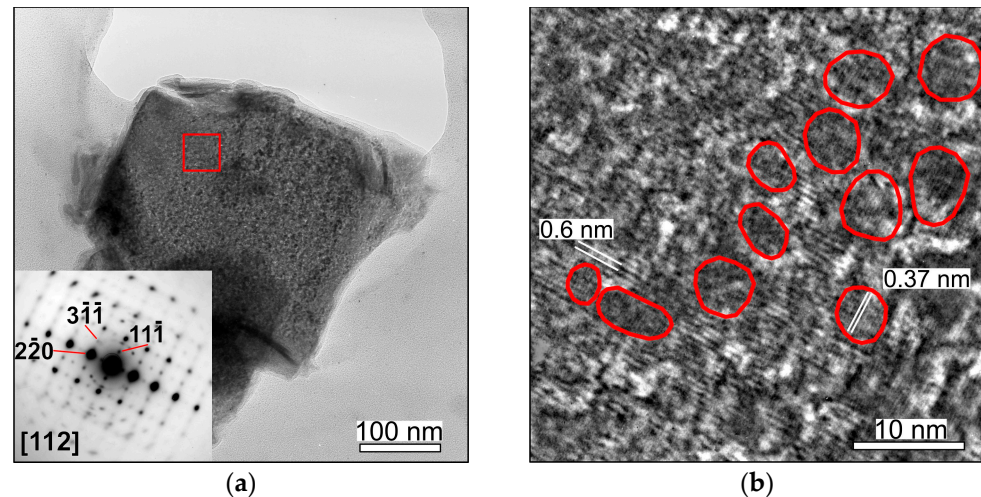


Figure 5. TEM study of hydroknoelsmoreite: (a) Morphology of hydroknoelsmoreite particle viewed along [112] (in insert: SAED pattern of the particle from zone [112]; red square contour outlines the region studied with HR TEM in Figure 5b); (b) HR TEM image of hydroknoelsmoreite viewed along [112] showing defect structure of the mineral.

A high-resolution (HR) image of the region in Figure 5a, outlined in red, shows the defect structure of the particle in phase contrast (Figure 5b). There are areas with well and hardly pronounced one- and two-dimensional lattice fringes corresponding to d-spacings 0.6 nm (11–1) and 0.37 nm (2–20) of the zone [112] of hydroknoelsmoreite. Some of the homogeneous areas (domains) with well-defined one-dimensional lattice fringes with a d-spacing of 0.37 nm are highlighted in red for a clearer visualization of the defect structure of the particle. As can be seen, homogenous domains are isometric, have a size of 3–7 nm, and correspond to the so-called “primary nanoparticles” before their coalescence to form a larger particle.

The results obtained are fully consistent with the mechanism of crystallization by particle attachment.

3.2. Preparation of W-Fe Pyrochlores in Laboratory Conditions at 70 °C

Two ways of synthesis of W-Fe pyrochlores were checked in the present study: (1) direct synthesis which has long been one of the most widely used methods for the synthesis of new tungsten oxide compounds [20,31]; (2) treatment of solid precursors with W-Fe solutions, which follows from the relationships of hydroknoelsmoreite and meymacite and their properties at the Grantcharitsa deposit. The latter process actually corresponds to the metasomatic transformation of meymacite into hydroknoelsmoreite.

3.2.1. Direct Hydrothermal Synthesis

Direct hydrothermal synthesis in the $\text{WO}_3\text{-Fe}_2\text{O}_3\text{-H}_2\text{O}$ system was carried out for two series of solutions, with an atomic Fe/W ratio of 0.1 and 0.5 (Figure 6a,b). These atomic ratios were initially chosen to (1) not exceed the upper limit of Fe/W in natural W-Fe

pyrochlores (~ 0.5); (2) to evaluate the possibility of crystallization of W-Fe pyrochlores at low Fe/W ratios of solutions.

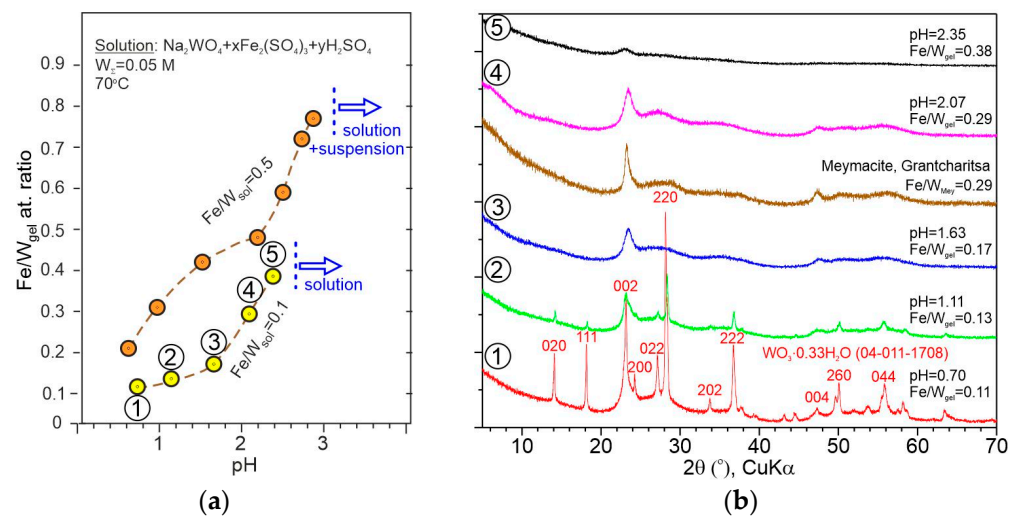


Figure 6. (a) Dependence of the Fe/W atomic ratio of solid precipitate on the Fe/W atomic ratio and pH of solutions (all pH measurements were performed at room temperature); (b) XRD patterns of solid precipitates obtained from solutions with Fe/W = 0.1 and different pH (samples 1, 2, 3, 4, and 5) and of meymacite from the Grantcharitsa deposit; (04-011-1708) is the reference code of the ICDD powder diffraction file (PDF) of orthorhombic $\text{WO}_3 \cdot 0.33\text{H}_2\text{O}$.

The experiments performed showed that no sample synthesized in the two series of experiments contained W-Fe pyrochlores. The resulting materials (gels) are highly disordered (X-ray amorphous), with the exception of two samples synthesized with a solution of Fe/W = 0.1 at pH = 0.7 and 1.11, containing a crystalline phase—orthorhombic $\text{WO}_3 \cdot 1/3\text{H}_2\text{O}$ (Fmm2) (Figure 6b). There is a steady increase in the atomic ratio of Fe/W in gels with an increasing pH of solutions: $\text{Fe}/\text{W}_{\text{gel}} = 0.21\text{--}0.77$ at $\text{pH} = 0.59\text{--}2.84$ for a solution with $\text{Fe}/\text{W} = 0.5$ and $\text{Fe}/\text{W}_{\text{gel}} = 0.11\text{--}0.38$ at $\text{pH} = 0.70\text{--}2.35$ for a solution with $\text{Fe}/\text{W} = 0.1$ (Figure 6a). At $\text{pH} > 3.1$ for a solution with $\text{Fe}/\text{W} = 0.5$ and $\text{pH} > 2.6$ for a solution with $\text{Fe}/\text{W} = 0.1$, no precipitates are formed.

It is noticeable that the XRD patterns of meymacite ($\text{Fe}/\text{W} = 0.29$) from the Grantcharitsa deposit and gels 3 ($\text{Fe}/\text{W} = 0.17$) and 4 ($\text{Fe}/\text{W} = 0.29$) are almost identical. The patterns of natural and artificial materials consist of two pronounced peaks at ~ 23 and $\sim 47^\circ$ (2θ) and several broad humps. The first peak of meymacite from the Grantcharitsa is narrower indicating better crystallinity of the natural material and better correspondence to reflection (002) of orthorhombic $\text{WO}_3 \cdot 1/3\text{H}_2\text{O}$ (Figure 6b).

3.2.2. Treatment of Solid Precursors with W-Fe Solutions

The experiments with the treatment of solid precursors with W-Fe solutions turned out to be very fruitful and, in our opinion, showed the most realistic path for the formation of W-Fe pyrochlores in the oxidation zone of deposits. This result is illustrated in Figure 7 by a diagram depicting the pH-concentration dependence of H_2SO_4 (mol/L) (blue curve) for a solution with $\text{Fe}/\text{W} = 0.11$. It has been established that 24 h at 70°C is sufficient time to achieve equilibrium in working solutions with $\text{Fe}/\text{W} = 0.11$ because, for different concentrations of H_2SO_4 , the measured pH values of solutions kept in a thermostat for different durations ≥ 24 h fall on the same curve. The lower part of the curve is directly related to Figure 6a, which shows pH ranges with and without precipitation for a solution of similar composition with $\text{Fe}/\text{W} = 0.1$. In essence, experiments involving solid precursor treatment are the next step in the development of direct hydrothermal synthesis. To solutions without precipitation (reactive solutions), we added in excess a solid compound containing W and Fe.

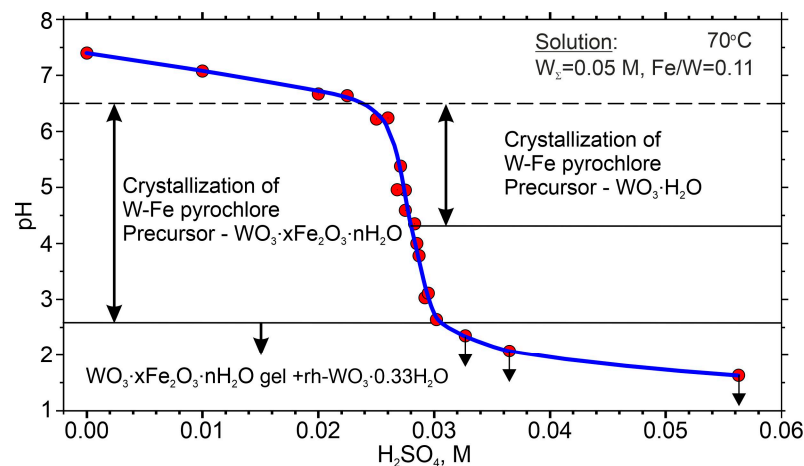


Figure 7. pH-H₂SO₄ (mol/L) dependence (blue curve) for a solution with Fe/W = 0.11; double arrows indicate the pH range of solutions at which they cause the formation of W-Fe pyrochlores during the treatment of WO₃·xFe₂O₃·nH₂O gels and WO₃·H₂O (tungstite); single arrows indicate the formation of precipitates in solutions; all pH measurements were performed at room temperature.

The obtained curve (Figure 7) is very close to the experimental titration curves for tungsten solutions [32,33], where the steepest part of the curve corresponds to the formation of different polytungstate ions. It is with the steepest part of the dependence of pH on the concentration of H₂SO₄ (mol/L) (pH ≈ 2.5–6.5) that the formation of W-Fe pyrochlores in our experiments is associated (Figure 7). It is noteworthy that the pH range of W-Fe solutions causing the formation of W-Fe pyrochlores is significantly narrower when using WO₃·H₂O as a precursor compared to WO₃·xFe₂O₃·nH₂O gels. The details of these experiments are presented below.

- Treatment of amorphous WO₃·xFe₂O₃·nH₂O with W-Fe solutions

Figure 8 shows the results of treating an initially amorphous gel with the composition WO₃·0.064Fe₂O₃·2H₂O with W-Fe solutions (Fe/W = 0.11, total W 0.05 mol/L, and pH 3.23–6.34) in thermostat 400 h. The formation of W-Fe pyrochlore occurs in all samples of the experimental batch.

Of all the experimental solutions, solution 3, whose initial pH₁ corresponds to the upper inflection point of the curve (pH-H₂SO₄) in Figure 8a, shows the largest decrease in pH (from pH₁ = 6.04 to pH₂ = 3.74). Namely, this solution provides the best conditions for the transformation of the amorphous gel into W-Fe pyrochlore, as evidenced by the XRD pattern in Figure 8b. The smallest decrease in pH is characteristic of solutions whose initial pH₁ is close to the lower inflection point, where gel precipitation occurs (Figures 7 and 8a). These solutions provide a weak transformation of the gel into W-Fe pyrochlore (Figure 8b). The formed W-Fe pyrochlores show an opposite trend in Fe/W variation with pH compared to that found for the gels (Figure 6a), namely the Fe/W of W-Fe pyrochlores increases from 0.15 to 0.33 at decreasing pH₂ from 5.35 to 3.74.

Well-faceted octahedral crystals 8–10 μm in size and their intergrowths according to the spinel law are more typical for samples with a low degree of conversion of gels into W-Fe pyrochlores (sample 1 in Figure 8a,b and its SEM image in Figure 9a). For comparison, Figure 9b shows crystals 1.5–2 μm in size obtained in the experiment with better conversion of gels into pyrochlore (Figure 8, solution and sample 3).

In addition to crystals with well-developed and smooth {111} faces, in almost all of the W-Fe pyrochlore samples we obtained, mosaic or grained surfaces of the {111} faces are observed, very similar to the surfaces of the {111} faces of natural hydrokenoelsmorite samples studied by us (Figure 4), which are the result of crystallization by particle attachment. All this indicates the uniformity of both the crystallization conditions and the crystallization mechanism of W-Fe pyrochlores under natural and laboratory conditions.

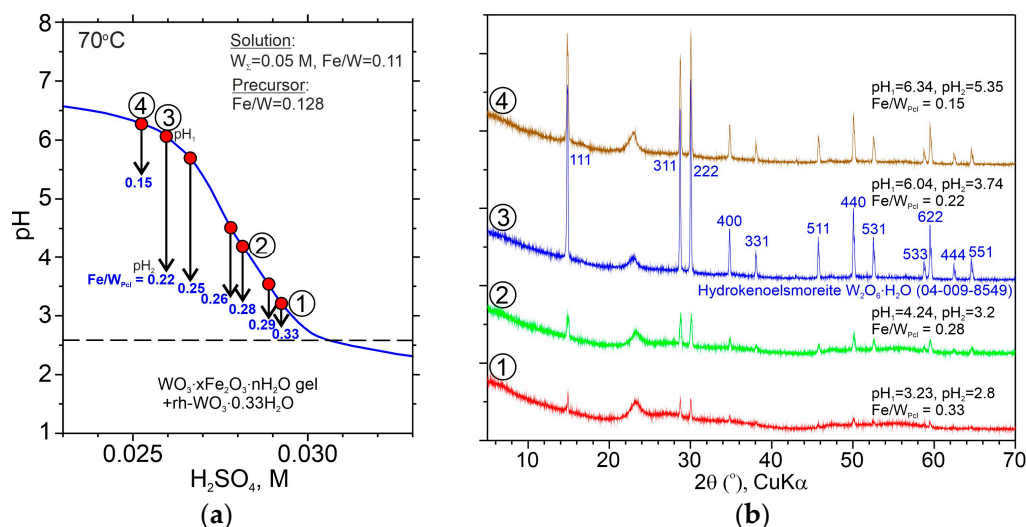


Figure 8. Formation of W-Fe pyrochlore as a result of treatment of amorphous gel ($Fe/W_{gel} = 0.128$) with solutions $Fe/W_{sol} = 0.11$ at different pH: (a) Details of the experiments: changes in the pH of the solutions after the experiments (indicated by arrows; pH_1 —before experiment; pH_2 —after the experiment) and variations in the Fe/W ratio of W-Fe pyrochlore (Fe/W_{Pcl}); (b) XRD patterns of samples 1–4 (also shown in Figure 8a), demonstrating different degrees of conversion of the amorphous gel into W-Fe pyrochlore depending on the initial pH (pH_1) of the working solution; indexation (sample 3) according to ICDD PDF 04-009-8549 of hydrokenoelsmoreite, $W_2O_6 \cdot H_2O$.

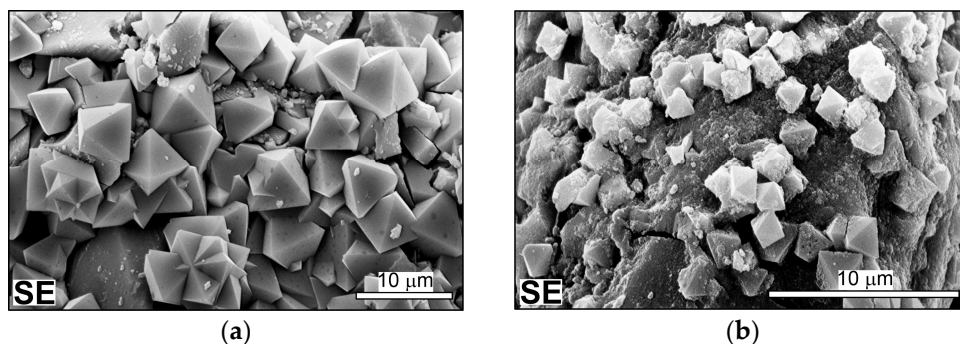


Figure 9. Octahedral crystals of W-Fe pyrochlore and their aggregates obtained by treatment of amorphous gel ($Fe/W_{gel} = 0.128$) with solutions ($Fe/W_{sol} = 0.11$): (a) sample and solution 1 in Figure 8: $Fe/W_{Pcl} = 0.33, pH_1 = 3.23, pH_2 = 2.8$; (b) sample and solution 3 in Figure 1: $Fe/W_{Pcl} = 0.22, pH_1 = 6.04, pH_2 = 3.74$.

Examples of such a surface of the {111} faces are presented in Figure 10.

In our experiments, in addition to W-Fe pyrochlores forming octahedral crystals, several samples of platy W-Fe pyrochlores were also obtained. Platy hydrokenoelsmoreite (ferritungstite) was first described by [7]. Since there is doubt that the author actually described platy crystals of jarosite, it can be considered that reliable platy crystals of ferritungstite were first described by Van Tassel [15] and later by Sahama [6]. Platy crystals of elsmoreite group minerals were later discovered in other deposits of the world [3,13].

Platy crystals of W-Fe pyrochlore were obtained by treating the initial amorphous gels $WO_3 \cdot xFe_2O_3 \cdot nH_2O$ with $Fe/W \leq 0.16$ with a solution ($Fe/W = 0, pH_1 \approx 3.2$). The result of such an experiment is shown in Figure 11. It is noteworthy that two gels of similar composition ($Fe/W = 0.16$ and 0.20) when interacting with the same solution give different final products—platy W-Fe pyrochlore (from the gel with $Fe/W = 0.16$) and octahedral W-Fe pyrochlore (from the gel with $Fe/W = 0.20$).

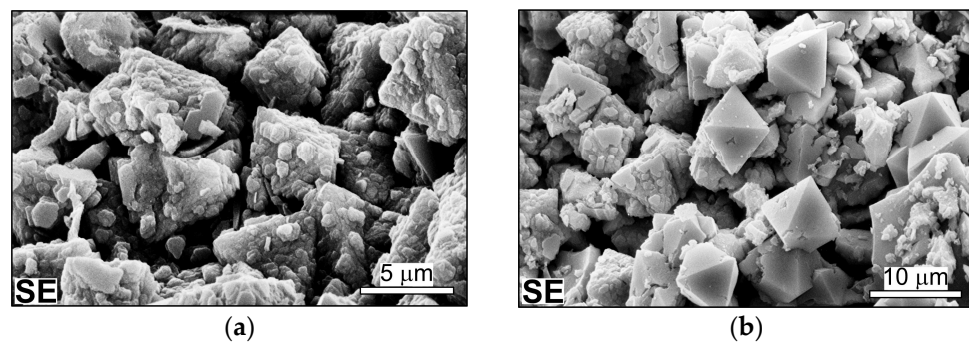


Figure 10. SEM images of W-Fe pyrochlore crystals whose {111} faces demonstrate granular (mosaic) structure as a result of crystallization by particle attachment [27,28]: (a) granular {111} faces, which are similar to the faces of natural hydrokenoelsmoreite from the Grantcharitsa deposit (Figure 4a); (b) smooth and rough (incomplete) surfaces of {111} faces. W-Fe pyrochlore: $Fe/W_{Pcl} = 0.26$; solution: $Fe/W = 0.11$, $pH_1 = 4.11$, $pH_2 = 3.21$; precursor: $Fe/W_{gel} = 0.099$.

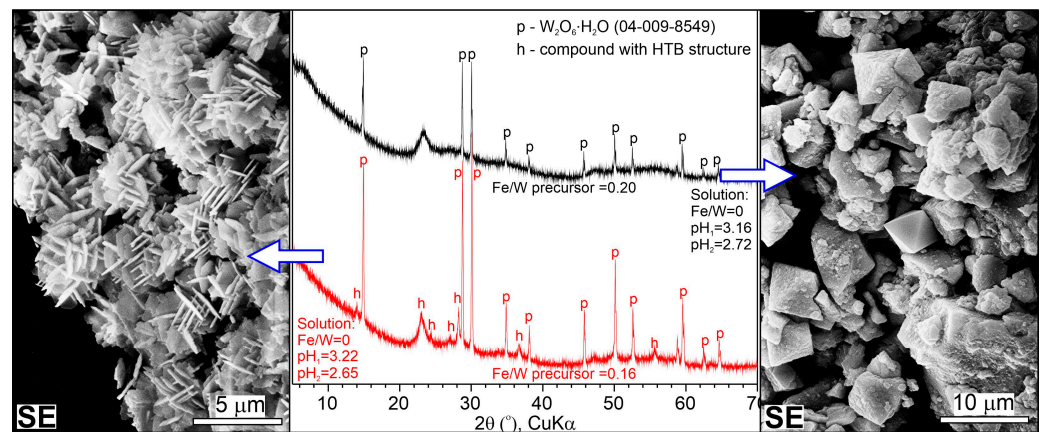


Figure 11. Platy (left, $Fe/W_{Pcl} = 0.17$) and octahedral (right, $Fe/W_{Pcl} = 0.28$) W-Fe pyrochlores formed after interaction of solution ($Fe/W = 0$, $pH_1 \approx 3.2$) with two precursors with $Fe/W = 0.16$ and 0.20 , respectively. The octahedral W-Fe pyrochlore on {111} faces exhibited distinct signs of crystallization by particle attachment.

Analysis of the XRD patterns of the two samples (Figure 11) shows that in addition to the platy W-Fe pyrochlore, a compound with a hexagonal tungsten bronze (HTB) structure is also formed from the gel with $Fe/W = 0.16$. The diffraction peaks of the compound match well with those of metastable hexagonal WO_3 [34] (ICDD PDF 04-007-0979) and sodium tungstate hydrates $Na_xWO_{3+x/2} \cdot zH_2O$ [35,36] (ICDD PDF 01-081-0577). Most likely, the presence of the HTB phase leads to the formation of platy W-Fe pyrochlore. Another significant difference between the two products is their composition: the Fe/W atomic ratio in the platy and octahedral W-Fe pyrochlore is 0.17 and 0.28, respectively.

- Treatment of $WO_3 \cdot H_2O$ with W-Fe solutions

The treatment of $WO_3 \cdot H_2O$ as a precursor with W-containing solutions shows the following:

(i) The interaction of Fe-free W solutions ($Fe/W = 0$) with $WO_3 \cdot H_2O$ does not lead to the formation of tungsten pyrochlore (Figure 12, the lower part of the figure; Figure 13a, XRD patterns 1 and 2). The only processes are dissolution, the formation of a small amount of tungsten hydrogen oxide, $H_{0.1}WO_3$ (ICDD PDF 00-023-1448), and at $pH > 6.5$, the formation of amorphous precipitates followed by complete dissolution.

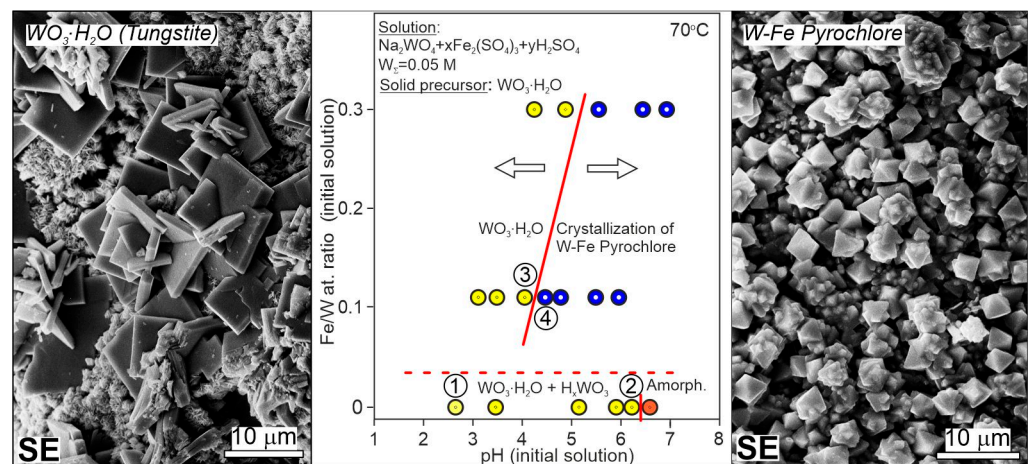


Figure 12. Conditions of crystallization of W-Fe pyrochlores after $\text{WO}_3 \cdot \text{H}_2\text{O}$ (tungstite). Samples 1, 2, 3, and 4 indicated on the graphs were examined using XRD analysis (Figure 13a). SEM images: on the left—sample 3 (tungstite); on the right—sample 4 (W-Fe pyrochlore).

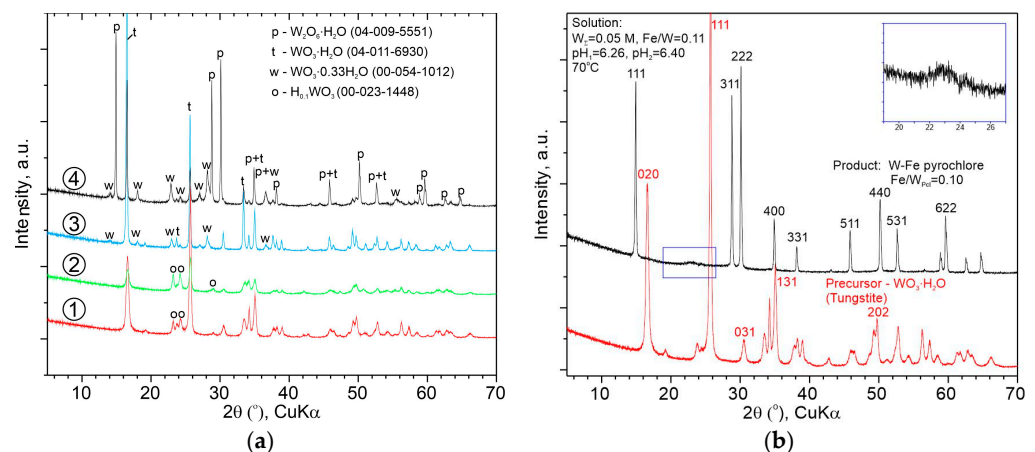


Figure 13. XRD patterns of products of treatment of $\text{WO}_3 \cdot \text{H}_2\text{O}$ with W-Fe solutions: (a) Series of XRD patterns of samples 1–4 in Figure 12. Samples 1 and 2 are after treatment with a solution with $\text{Fe}/\text{W} = 0$. Samples 3 and 4 are after treatment with a solution with $\text{Fe}/\text{W} = 0.11$. $\text{WO}_3 \cdot \text{H}_2\text{O}$ with traces of orthorhombic $\text{WO}_3 \cdot 0.33\text{H}_2\text{O}$ obtained via sulfuric acid decomposition of scheelite is used as a precursor for samples 3 and 4. (b) XRD pattern of precursor ($\text{WO}_3 \cdot \text{H}_2\text{O}$ obtained by the method of Freedman [22]) and its product—W-Fe pyrochlore and low-crystalline (X-ray amorphous) material corresponding to natural meymacite.

(ii) The formation of W-Fe pyrochlore occurs only in the presence of Fe^{3+} in the working solution (in our experiments, we used working solutions with a Fe/W ratio of 0.11 and 0.3). There are clear threshold pH values of working solutions, above which they cause the formation of W-Fe pyrochlore: $\text{pH} = 4.3$ for solutions with $\text{Fe}/\text{W} = 0.11$ and $\text{pH} = 5.2$ for solutions with $\text{Fe}/\text{W} = 0.3$ (Figures 12 and 13a, samples 3 and 4).

(iii) Crystallization of W-Fe pyrochlore upon treatment of $\text{WO}_3 \cdot \text{H}_2\text{O}$ with a W-Fe solution ($\text{Fe}/\text{W} = 0.11$) is accompanied by the formation of highly disordered material corresponding to meymacite and gels obtained via direct hydrothermal synthesis (Figure 6b).

3.2.3. Chemical Composition, Crystal Chemistry and Conditions of Crystallization of W-Fe Pyrochlores

Data on the chemical composition of experimentally obtained W-Fe pyrochlores are summarized in Figure 14 in the form of the dependence of the Fe/W atomic ratio in pyrochlore on the pH of solutions, as well as in the form of representative EDX analyses of

W-Fe pyrochlores and their crystal chemical formulas in Table 2. To plot the experimental points in the $\text{Fe}/\text{W}_{\text{pchl}}-\text{pH}$ coordinates in Figure 14, we used pH_2-pH measured after the experiment as an approximation to equilibrium. The figure also shows the distribution areas of octahedral and platy crystals of W-Fe pyrochlore.

The composition of W-Fe pyrochlore is the result of the integrated influence of several factors: the composition of the precursor, and the composition and pH of the aqueous solution. Depending on the weight of each of these factors, we conditionally divided all synthesized pyrochlores into four groups (I–IV).

Group I includes W-Fe pyrochlores obtained using $\text{WO}_3 \cdot \text{H}_2\text{O}$ as a precursor. This group is characterized by a similar composition ($\text{Fe}/\text{W} = 0.11-0.08$) and relative independence from all the factors specified above. Important for this group is the presence of Fe^{3+} in the solution.

Group II includes W-Fe pyrochlores obtained by treating various precursors with Fe/W from 0.06 to 0.20 with almost the same solution ($\text{Fe}/\text{W} = 0$, $\text{pH}_2 \approx 2.7-2.8$). This group shows a very strong dependence on the composition of the precursor.

Groups III and IV show dependence on all factors, but mainly on Fe/W and pH of the aqueous solution. These two groups are characterized by a clear increase in the Fe/W of pyrochlore with decreasing pH (Figure 14). According to the data for the two solutions we used with Fe/W equal to 0.11 and 0.5, respectively, with increasing Fe/W of the solution, the dependence of the pyrochlore composition on the pH of the solution decreases. It seems that these two groups correspond well to $(\text{Fe} + \text{Al})/\text{W}$ atomic ratios of natural members of the elsmoreite group minerals.

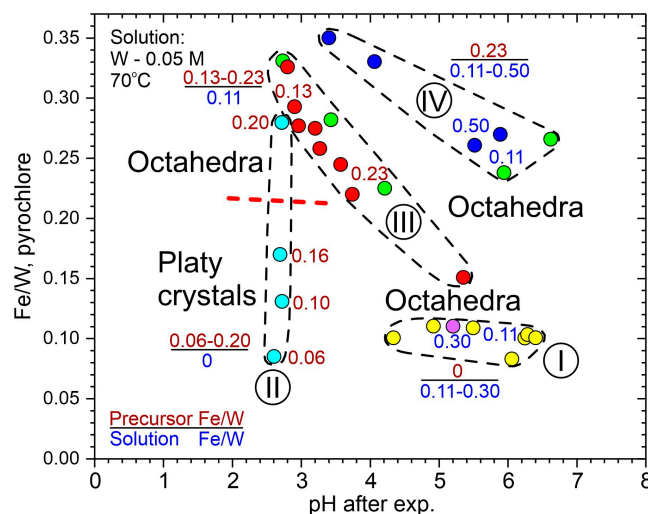


Figure 14. Composition distribution (in terms of Fe/W atomic ratio) of artificial W-Fe pyrochlores depending on pH, aqueous solution composition, and precursor composition. The groups separated (I–IV) reflect the weight of these factors. Distribution of various morphological types of W-Fe pyrochlore—octahedral and platy.

In addition to WO_3 and Fe_2O_3 , the W-Fe pyrochlores we obtained also contain Na_2O and H_2O (Table 2). The presence of Na_2O was expected since sodium tungstate dihydrate $\text{Na}_2\text{WO}_4 \cdot 2\text{H}_2\text{O}$ was used to prepare tungstate solutions. The incorporation of Na into the structure of the W-Fe pyrochlores obtained by us is not associated with the incorporation of Fe into the W positions and charge compensation. The Na_2O content in W-Fe pyrochlores increases with increasing pH while the Fe_2O_3 content decreases. The H_2O content in the W-Fe pyrochlores was estimated as the difference between 100% and the sum of the analysis and this content was then used for the calculation of crystal chemical formulas. According to the calculated crystal chemical formulas and according to the existing nomenclature of the pyrochlore supergroup of minerals [1] obtained by us, W-Fe pyrochlores can be classified as hydrokenoelsmoreite (analyses 1 and 2 in Table 2), “hydroelsmoreite” (anal-

yses 3–6), and “hydronatroelsmoreite” (analyses 7–9). The names “hydroelsmorite” and “hydronatroelsmorite” are put in quotation marks because minerals under these names have not yet been found.

Table 2. Representative EDX analyses of W-Fe pyrochlores obtained by treatment of precursors with Fe/W = 0–0.23 by a solution with Fe/W = 0.11 at different pH (wt.%, polished samples).

Nº an.	Fe/W Precursor	pH ₁	pH ₂	WO ₃	Fe ₂ O ₃	Na ₂ O	H ₂ O ¹	Fe/W at. Ratio
1	0.13	3.23	2.80	80.16	9.01	3.14	7.69	0.33
2	0.13	4.24	3.20	80.41	7.58	4.07	7.94	0.28
3	0.13	6.04	3.74	80.63	6.11	5.15	8.1	0.22
4	0.13	6.34	5.35	82.45	4.28	5.29	7.98	0.15
5	0.23	2.86	2.73	78.36	8.93	3.68	9.03	0.33
6	0.23	5.14	4.21	80.03	6.19	6.07	7.71	0.23
7	0.23	6.65	6.62	79.0	7.23	6.27	7.50	0.27
8	0	6.26	5.51	86.9	3.2	5.71	4.21	0.11
9	0	6.26	6.04	87.45	2.46	5.38	4.71	0.08

Crystal chemical formulas/nomenclature names

1. $(\square_{1.213}\text{Na}_{0.442}(\text{H}_2\text{O})_{0.345})_{\Sigma 2}(\text{W}_{1.508}\text{Fe}^{3+}_{0.492})_{\Sigma 2}(\text{O}_{4.967}(\text{OH})_{1.033})_{\Sigma 6}(\text{H}_2\text{O})$ /Hydroknoelsmoreite
2. $(\square_{0.757}\text{Na}_{0.595}(\text{H}_2\text{O})_{0.648})_{\Sigma 2}(\text{W}_{1.570}\text{Fe}^{3+}_{0.430})_{\Sigma 2}(\text{O}_{5.306}(\text{OH})_{0.694})_{\Sigma 6}(\text{H}_2\text{O})$ /Hydroknoelsmoreite
3. $(\text{H}_2\text{O})_{0.969}\text{Na}_{0.783}\square_{0.248})_{\Sigma 2}(\text{W}_{1.639}\text{Fe}^{3+}_{0.361})_{\Sigma 2}(\text{O}_{5.700}(\text{OH})_{0.300})_{\Sigma 6}(\text{H}_2\text{O})$ /"Hydroelsmoreite"
4. $(\text{H}_2\text{O})_{1.166}\text{Na}_{0.834})_{\Sigma 2}(\text{W}_{1.738}\text{Fe}^{3+}_{0.262})_{\Sigma 2}(\text{O}_{6.000})_{\Sigma 6}((\text{H}_2\text{O})_{0.952}(\text{OH})_{0.048})_{\Sigma 1}$ /"Hydroelsmoreite"
5. $(\text{H}_2\text{O})_{0.744}\square_{0.728}\text{Na}_{0.528})_{\Sigma 2}(\text{W}_{1.502}\text{Fe}^{3+}_{0.498})_{\Sigma 2}(\text{O}_{5.033}(\text{OH})_{0.967})_{\Sigma 6}(\text{H}_2\text{O})$ /"Hydroelsmoreite"
6. $(\text{H}_2\text{O})_{0.938}\text{Na}_{0.927}\square_{0.135})_{\Sigma 2}(\text{W}_{1.633}\text{Fe}^{3+}_{0.367})_{\Sigma 2}(\text{O}_{5.827}(\text{OH})_{0.173})_{\Sigma 6}(\text{H}_2\text{O})$ /"Hydroelsmoreite"
7. $(\text{Na}_{0.938}(\text{H}_2\text{O})_{0.770}\square_{0.292})_{\Sigma 2}(\text{W}_{1.580}\text{Fe}^{3+}_{0.420})_{\Sigma 2}(\text{O}_{5.679}(\text{OH})_{0.321})_{\Sigma 6}(\text{H}_2\text{O})$ /"Hydronatroelsmoreite"
8. $(\text{Na}_{0.889}\square_{0.829}(\text{H}_2\text{O})_{0.282})_{\Sigma 2}(\text{W}_{1.807}\text{Fe}^{3+}_{0.193})_{\Sigma 2}(\text{O}_{6.000})_{\Sigma 6}((\text{H}_2\text{O})_{0.689}(\text{OH})_{0.311})_{\Sigma 1}$ /"Hydronatroelsmoreite"
9. $(\text{Na}_{0.848}\square_{0.673}(\text{H}_2\text{O})_{0.479})_{\Sigma 2}(\text{W}_{1.849}\text{Fe}^{3+}_{0.151})_{\Sigma 2}(\text{O}_{6.000})_{\Sigma 6}((\text{H}_2\text{O})_{0.605}(\text{OH})_{0.395})_{\Sigma 1}$ /"Hydronatroelsmoreite"

¹ The difference between 100% and the sum of the analysis.

The calculated unit cell parameters (for S.G. Fd-3m) of the resulting W-Fe pyrochlores range from 10.28 to 10.32 Å, which corresponds to the parameters of natural and artificial W-Fe pyrochlores.

4. Discussion

Natural materials (secondary minerals from the Grantcharitsa deposit, Bulgaria) and laboratory experiments show that the treatment (metasomatic alteration) of low-crystalline compounds such as $\text{WO}_3 \cdot x\text{Fe}_2\text{O}_3 \cdot n\text{H}_2\text{O}$ with an aqueous solution containing W and Fe^{3+} is an effective and simple method for obtaining artificial W-Fe pyrochlores. In our experiments, there are several sources of the substance for the formation of W-Fe pyrochlore, which predetermine the mechanism of pyrochlore crystallization:

(1) W and Fe ions in solution. In its pure form, this source of the substance is presented in group I of pyrochlores in Figure 14 (precursor— $\text{WO}_3 \cdot \text{H}_2\text{O}$; solutions: Fe/W = 0.11 and 0.3; pH 4.2–6.6; Fe/W pyrochlore = 0.08–0.11). The composition of W-Fe pyrochlore corresponds well to the iron (III) heteropolytungstate ion of the Keggin-type: $[\text{Fe}^{3+}_4\text{O}_4\text{W}_{12}\text{O}_{36}]^{5-}$ (Fe/W = 1/12 = 0.083) [37].

(2) W and Fe from the precursor. Group II of pyrochlores in Figure 14 corresponds most closely to the influence factor of the precursor composition (at constant pH and composition of solution).

(3) This source of W and Fe is highly dependent on the pH of the solution. The source is not obvious, but it is what determines the increase in the Fe/W ratio in pyrochlores with decreasing pH (groups III and IV in Figure 14). The experiment on direct hydrothermal synthesis in the $\text{WO}_3\text{-Fe}_2\text{O}_3\text{-H}_2\text{O}$ system (Figure 6a) suggests that this source is colloidal particles or nanoparticles $(\text{W,Fe})(\text{O,OH})_3 \cdot n\text{H}_2\text{O}$ (Fe/W = 0.4 for a solution with Fe/W = 0.11) (Figure 6a). Some of these particles are visible as a suspension.

Combination and interaction of these sources cause the pathway for the crystallization of W-Fe pyrochlores, including the formation of pyrochlore nanoparticles ~5 nm and

their further oriented attachment on the growing {111} faces of artificial and natural W-Fe pyrochlores (Figure 15).

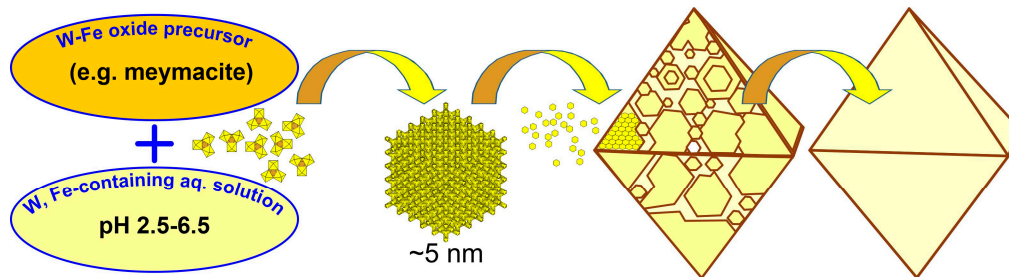


Figure 15. Model of the mechanism of crystallization of artificial and natural W-Fe pyrochlores by oriented particle attachment on the growing {111} face.

Experiments conducted with different precursors show some significant differences. The best results were obtained using $WO_3 \cdot xFe_2O_3 \cdot nH_2O$ gels, which are artificial amorphous analogs of meymacite. For $WO_3 \cdot H_2O$ (tungstite), the pH range of the working solution causing the formation of W-Fe pyrochlore is significantly narrower (Figures 12 and 16). The reason for this behavior can be sought in the thermodynamics of crystallization and dissolution of tungstite. There are indications that when $WO_3 \cdot H_2O$ is treated with W-Fe solutions, an intermediate product is formed—a low-crystalline analog of meymacite (Figure 13b). It is this product that most likely plays the role of a precursor for the formation of W-Fe pyrochlore.

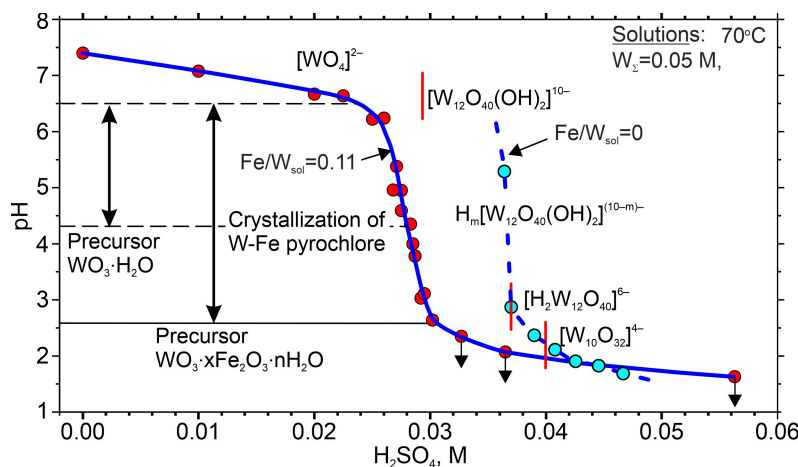


Figure 16. pH- H_2SO_4 (mol/L) curves for solutions with $Fe/W = 0.11$ (solid blue line) and $Fe/W = 0$ (dotted blue line); polytungstate ions are shown for a solution with $Fe/W = 0$.

In Figure 16, for comparison purposes, two pH- H_2SO_4 (mol/L) curves are presented—for $Fe/W = 0.11$ and $Fe/W = 0$, respectively.

For the pure tungstate system, the formation of polytungstate ions is described as a protonation of monomeric ion WO_4^{2-} : $p[WO_4]^{2-} + qH^+ = [WO_4]^{2-p}(H^+)_q$, $z = q/p$ —degree of protonation [38]. In Figure 16, the vertical red lines corresponding to z show paratungstate $[W_{12}O_{40}(OH)_2]^{10-}$ ($z = 1.17$) (+protonated forms), metatungstate $[H_2W_{12}O_{40}]^{6-}$ ($z = 1.50$), and tungstate-Y $[W_{10}O_{32}]^{4-}$ ($z = 1.60$). Formally, the pH range of solutions with $Fe/W = 0.11$, which causes the formation of W-Fe pyrochlores after $WO_3 \cdot xFe_2O_3 \cdot nH_2O$ gels, almost completely coincides with the range in which paratungstate ions dominate in solutions with $Fe/W = 0$. The role of para- and metatungstates in the crystallization of W-Fe pyrochlore, however, can only be discussed for experiments with $Fe/W_{sol} = 0$. This, for example, is the case of samples with platy W-Fe pyrochlores, containing compounds with a hexagonal tungsten bronze structure (Figure 11), formed in the pH range 3.2–2.6,

where both paratungstate and metatungstate ions are present (Figure 16). It is expected that it is the metatungstate ion that promotes the formation of the hexagonal phase. It is possible that under such conditions, two secondary tungsten minerals with a mixed pyrochlore–hexagonal tungsten bronze structure are formed—phyllostungstite [39] and pittongite [40].

Apparently, low-crystalline minerals such as meymacite play a significant role as a precursor in the crystallization of elsmoreite group minerals. There are some indications (a broad peak at the place of (001) reflection of hexagonal WO_3 (ICDD PDF 04-007-0979) in the synchrotron powder pattern) that the mineral pittongite [40] is a product of the alteration of meymacite. Another possible candidate precursor for the formation of elsmoreite group minerals is anthoinite $\text{AlWO}_3(\text{OH})_3$. In addition to the formation of pseudomorphs after scheelite, anthoinite often occurs together with hydrokenoelsmoreite (formal alumo-tungstite and ferritungstite) [2,6,14].

Supplementary Materials: The following supporting information can be downloaded at: <https://www.mdpi.com/article/10.3390/min14040422/s1>, Table S1: Preparation of amorphous W-Fe oxide hydrate gels $\text{WO}_3 \cdot x\text{Fe}_2\text{O}_3 \cdot n\text{H}_2\text{O}$ at room temperature.

Author Contributions: Conceptualization, M.T.; methodology, M.T. and E.T.; validation, M.T. and E.T.; formal analysis, M.T.; investigation, M.T. and E.T.; resources, M.T.; writing—original draft preparation, M.T.; visualization, M.T. and E.T.; supervision, M.T.; project administration, M.T.; funding acquisition, M.T. All authors have read and agreed to the published version of the manuscript.

Funding: This research was funded by the Bulgarian National Science Fund (BNSF), grant number KP-06-OPR 03/5, 2018.

Data Availability Statement: Data are contained within the article and supplementary materials.

Acknowledgments: The authors acknowledge the technical support from the project PERIMED BG05M2OP001-1.002-0005/29.03.2018 (2018–2023).

Conflicts of Interest: The authors declare no conflicts of interest.

References

- Atencio, D.; Andrade, M.B.; Christy, A.G.; Giere, R.; Kartashov, P.M. The pyrochlore supergroup of minerals: Nomenclature. *Can. Mineral.* **2010**, *48*, 569–594. [[CrossRef](#)]
- Ercit, T.S.; Robinson, G.W. A refinement of the structure of ferritungstite from Kalzas mountain, Yukon, and observations on the tungsten pyrochlores. *Can. Mineral.* **1994**, *32*, 567–574.
- Mills, S.; Christy, A.G.; Kampf, A.R.; Birch, W.D.; Kasatkin, A. Hydroxykenoelsmoreite, the first new mineral from the Republic of Burundi. *Eur. J. Mineral.* **2017**, *29*, 491–497. [[CrossRef](#)]
- Williams, P.; Leverett, P.; Sharpe, J.L.; Colchester, D.M.; Rankin, J. Elsmoreite, cubic $\text{WO}_3 \cdot 0.5\text{H}_2\text{O}$, a new mineral species from Elsmore, New South Wales, Australia. *Can. Mineral.* **2005**, *43*, 1061–1064. [[CrossRef](#)]
- Yuan, X.; Ningyue, S.; Guowu, L.; Guangming, Y. Hydroplumboelsmoreite, $(\text{Pb}_1\Box_1)_{\Sigma 2}(\text{W}_{1.33}\text{Fe}^{3+}_{0.67})_{\Sigma 2}\text{O}_6(\text{H}_2\text{O})$, a redefined mineral species of the elsmoreite group from China. *Mineral. Mag.* **2021**, *85*, 890–900. [[CrossRef](#)]
- Sahama, T.G. The secondary tungsten minerals—A review. *Mineral. Rec.* **1981**, *12*, 81–87.
- Schaller, W.T. Ferritungstite, a new mineral. *Am. J. Sci.* **1911**, *32*, 161–162. [[CrossRef](#)]
- Kerr, P.F. *Tungsten Mineralization in the United States*; Geological Society of America Memoirs: Boulder, CO, USA, 1946; Volume 15, pp. 1–226. [[CrossRef](#)]
- Richter, D.H.; Reichen, L.E.; Lemmon, D.M. New Data on ferritungstite from Nevada. *Am. Min.* **1957**, *42*, 83–90.
- Matsubara, S.; Kato, A.; Tiba, T. Ferritungstite from the Nita Mine, Yaku Island Kagoshima Prefecture, Japan. *Bull. Nat. Sci. Mus. Tokio Ser. C* **1994**, *20*, 45–51.
- Kempe, U.K.; Sorokin, N.D. On the wolframite replacement processes. *Dokl. Akad. Nauk SSSR* **1988**, *303*, 203–206. (In Russian)
- Tarassov, M.P.; Marinov, M.S.; Konstantinov, L.L.; Zotov, N.S. Raman spectroscopy of ferritungstite: Experimental and model spectra. *Phys. Chem. Miner.* **1994**, *21*, 63–66. [[CrossRef](#)]
- Mills, S.J.; Christy, A.G.; Rumsey, M.S.; Spratt, J. The crystal chemistry of elsmoreite from the Hemerdon (Drakelands) mine, UK: Hydrokenoelsmoreite-3C and hydrokenoelsmoreite-6R. *Mineral. Mag.* **2016**, *80*, 1195–1203. [[CrossRef](#)]
- Shimobayashi, N.; Ohnishi, M.; Tsuruta, K. Secondary tungsten minerals in quartz veins in the Ishidera area, Wazuka, Kyoto Prefecture, Japan: Anthoinite, mpororoite, and Fe-free hydrokenoelsmoreite. *J. Mineral. Petrol. Sci.* **2012**, *107*, 33–38. [[CrossRef](#)]
- Van Tassel, R. Ferritungstite et meymacite de Meymac, France, et d’Afrique centrale. *Bull. Soc. Belge Geol. Paleontol. d’Hydrol.* **1961**, *LXX*, 376–399.

16. Tarassov, M.P.; Tarassova, E.D. Structural and chemical evolution of mineral forms of tungsten in the oxidation zone of the Grantcharitza deposit (Western Rhodopes, Bulgaria). *Bulg. Chem. Commun.* **2018**, *50*, 270–280.
17. Guo, J.; Li, Y.J.; Whittingham, M.S. Hydrothermal synthesis of electrode materials Pyrochlore tungsten trioxide film. *J. Power Sources* **1995**, *54*, 461–464. [[CrossRef](#)]
18. Ravi, G.; Palla, S.; Veldurthi, N.K.; Reddy, J.R.; Vithal, M. Solar water-splitting with the defect pyrochlore type of oxides $KFe_{0.33}W_{1.67}O_6$ and $Sn_{0.5}Fe_{0.33}W_{1.67}O_6 \cdot xH_2O$. *Int. J. Hydrogen Energy* **2014**, *39*, 15352–15361. [[CrossRef](#)]
19. Jitta, R.R.; Gundeboina, R.; Veldurthi, N.K.; Guje, R.; Muga, V. Defect pyrochlore oxides: As photocatalyst materials for environmental and energy applications—A review. *J. Chem. Technol. Biotechnol.* **2015**, *90*, 1937–1948. [[CrossRef](#)]
20. Günter, J.R.; Amberg, M.; Schmalle, H. Direct synthesis and single crystal structure determination of cubic pyrochlore-type tungsten trioxide hemihydrate, $WO_3 \cdot 0.5H_2O$. *Mater. Res. Bull.* **1989**, *24*, 289–292. [[CrossRef](#)]
21. Pope, M.T. *Heteropoly and Isopoly Oxometalates*; Springer: Berlin/Heidelberg, Germany, 1983; 180p.
22. Freedman, M.L. The tungstic acids. *J. Am. Chem. Soc.* **1959**, *81*, 3834–3839. [[CrossRef](#)]
23. Pierrot, R.; van Tassel, R. Nouvelle définition de la meymacite et nomenclature des «acides tungstiques» naturels. *Bull. Soc. Franç. Minér. Crist.* **1965**, *88*, 613–617. [[CrossRef](#)]
24. Gerand, B.; Nowogrocki, G.; Figlarz, D.M. A new tungsten trioxide hydrate, $WO_3 \cdot 1/3H_2O$: Preparation, characterization, and crystallographic study. *J. Solid State Chem.* **1981**, *38*, 312–320. [[CrossRef](#)]
25. Scherer, G.W. Aging and drying of gels. *J. Non-Cryst. Solids* **1988**, *100*, 77–92. [[CrossRef](#)]
26. Smirnov, S.S. *The Oxidation Zone of Sulfide Deposits*; USSR Academy of Sciences Publishing House, USSR: Moscow, Russia, 1951; 334p. (In Russian)
27. De Yoreo, J.J.; Gilbert, P.U.; Sommerdijk, N.A.; Penn, R.L.; Whitelam, S.; Joester, D.; Zhang, H.; Rimer, J.D.; Navrotsky, A.; Banfield, J.F.; et al. Crystallization by particle attachment in synthetic, biogenic, and geologic environments. *Science* **2015**, *349*, aaa6760. [[CrossRef](#)] [[PubMed](#)]
28. Ivanov, V.K.; Fedorov, P.P.; Baranchikov, A.Y.; Osiko, V.V. Oriented attachment of particles: 100 years of investigations of non-classical crystal growth. *Russ. Chem. Rev.* **2014**, *83*, 1204–1222. [[CrossRef](#)]
29. Sonia, A.; Djaoued, Y.; Subramanian, B.; Jacques, R.; Eric, M.; Ralf, B.; Achour, B. Synthesis and characterization of novel nanorod superstructures and twin octahedral morphologies of WO_3 by hydrothermal treatment. *Mater. Chem. Phys.* **2012**, *136*, 80–89. [[CrossRef](#)]
30. Olliges-Stadler, I.; Rossell, M.D.; Süess, M.J.; Ludi, B.; Bunk, O.; Pedersen, J.S.; Birkedal, H.; Niederberger, M. A comprehensive study of the crystallization mechanism involved in the nonaqueous formation of tungstite. *Nanoscale* **2013**, *5*, 8517–8525. [[CrossRef](#)]
31. Reis, K.P.; Ramanan, A.; Whittingham, M.S. Hydrothermal synthesis of sodium tungstates. *Chem. Mater.* **1990**, *2*, 219–221. [[CrossRef](#)]
32. Barré, T.; Arurault, L.; Sauvage, F.X. Chemical behavior of tungstate solutions. Part 1. A spectroscopic survey of the species involved. *Spectrochim. Acta-A Mol. Biomol. Spectrosc.* **2005**, *61*, 551–557. [[CrossRef](#)]
33. Radio, S.V.; Kryuchkov, M.A.; Zavalova, E.G.; Baumer, V.N.; Shishkin, O.V.; Rozantsev, G.M. Equilibrium in the acidified aqueous solutions of tungstate anion: Synthesis of Co (II) isopolytungstates. Crystal structure of Co (II) paratungstate $B Co_5[W_{12}O_{40}(OH)_2] \cdot 37H_2O$. *J. Coord. Chem.* **2010**, *63*, 1678–1689. [[CrossRef](#)]
34. Gerand, B.; Nowogrocki, G.; Guenot, J.; Figlarz, M. Structural study of a new hexagonal form of tungsten trioxide. *J. Solid State Chem.* **1979**, *29*, 429–434. [[CrossRef](#)]
35. Reis, K.P.; Ramanan, A.; Whittingham, M.S. Synthesis of novel compounds with the pyrochlore and hexagonal tungsten bronze structures. *J. Solid State Chem.* **1992**, *96*, 31–47. [[CrossRef](#)]
36. Kumagai, N.; Matsuura, Y.; Umetzu, Y.; Tanno, K. Preparation and characterization of tungstic acid C phases containing various cations. *Solid State Ion.* **1992**, *53*, 324–332. [[CrossRef](#)]
37. Weiner, H.; Lunk, H.J.; Stösser, R.; Lück, R. Synthese, Charakterisierung und EPR-spektroskopische Untersuchung von Heteropolyverbindungen mit tetraedrisch bzw. oktaedrisch koordiniertem Eisen (III). *Z. Anorg. Allg. Chem.* **1989**, *572*, 164–174. [[CrossRef](#)]
38. Cruywagen, J.J. Protonation, oligomerization, and condensation reactions of vanadate (V), molybdate (VI), and tungstate (VI). In *Advances in Inorganic Chemistry*; Academic Press: Cambridge, MA, USA, 1999; Volume 49, pp. 127–182. [[CrossRef](#)]
39. Grey, I.E.; Mumme, W.G.; MacRae, C.M. Lead-bearing phyllostungstite from the Clara mine, Germany with an ordered pyrochlore-hexagonal tungsten bronze intergrowth structure. *Mineral. Mag.* **2013**, *77*, 57–67. [[CrossRef](#)]
40. Birch, W.D.; Grey, I.E.; Mills, S.J.; Bougerol, C.; Pring, A.; Ansermet, S. Pittongite, a new tungstate with a mixed-layer, pyrochlore-hexagonal tungsten bronze structure, from Victoria, Australia. *Can. Mineral.* **2007**, *45*, 857–864. [[CrossRef](#)]

Disclaimer/Publisher's Note: The statements, opinions and data contained in all publications are solely those of the individual author(s) and contributor(s) and not of MDPI and/or the editor(s). MDPI and/or the editor(s) disclaim responsibility for any injury to people or property resulting from any ideas, methods, instructions or products referred to in the content.